tahedral $V(CO)_6$, the V–C and C–O bond lengths were taken to be 2.001 and 1.128 Å, respectively, from published X-ray data.[44] The structures used for pentacoordinate $Mn(CO)_5$ were idealized D_{3h} and C_{4v} geometries; the C_{4v} structure for $Mn(CO)_5$ was taken to have a CO_{basal}–Mn–CO_{basal} angle of 164°, on the basis of previous experimental observations[29a] and theoretical considerations.[26b,31] The Mn–C and C–O bond distances were taken to be 1.855 and 1.129 Å, respectively, from the published X-ray data of $Mn_2(CO)_{10}$.[45] The Co–C and C–O bond lengths used for $Co(CO)_4$ in the ideal tetrahedral geometry were 1.797 and 1.168 Å on the basis of the X-ray data for $Co_2(CO)_8$.[46]

For all the electronic structure calculations of the hypothetical models for 19e transition states, a coordinate system was used such that PH_3 approached the metal center along the z axis. The metal carbonyl complex was rotated in space to provide for nucleophilic attack by PH_3 at the appropriate edge or face of the polyhedron such that the xz plane always functioned as a plane of symmetry, allowing for easy comparison of the contour maps generated. The relative orbital energies for calculations at different metal–nucleophile distances can vary by ±0.5 eV from errors in the numerical integration scheme. Therefore, the Walsh diagrams were constructed by using a core orbital of oxygen on the remote carbonyl ligands as an internal reference to compare orbital energies vs metal–nucleophile distance. The success of this procedure is evident in Figure 2 where the noninteracting 12e orbital energy remains constant while the energies of the interacting $10a_1$ and $11a_1$ orbitals vary considerably.

Acknowledgment. This material was based on work supported by the National Science Foundation (Grant CHE-85-04088). We thank Dr. Michael S. Greenfield for helpful discussions.

Registry No. PH_3, 7803-51-2; $V(CO)_6$, 14024-00-1; $Co(CO)_4$, 58207-38-8; $Mn(CO)_5$, 15651-51-1.

Supplementary Material Available: Tables of atomic character of frontier orbitals (24 pages). Ordering information is given on any current masthead page.

(45) Churchill, M. R.; Amoh, K. N.; Wasserman, H. J. *Inorg. Chem.* **1981**, *20*, 1609.
(46) Sumner, G. G.; Klug, H. P.; Alexander, L. E. *Acta Crystallogr.* **1964**, *17*, 732.

Empirical Potential Energy Surfaces Relating Structure and Activation Energy. 1. Metallacyclopentene Ring Inversion in (*s-cis*-η^4-Butadiene)metallocene Complexes and Related Compounds

Hans-Beat Bürgi* and Katharina C. Dubler-Steudle

Contribution from the Laboratory for Chemical and Mineralogical Crystallography, University of Berne, CH-3012 Berne, Switzerland. *Received June 23, 1987*

Abstract: X-ray structural data for (*s-cis*-η^4-butadiene)metallocene complexes and activation barriers for metallacyclopentene ring inversion in these compounds were retrieved from the literature and analyzed by principal-component analysis. It is found that the metallacyclopentene rings can be arranged into a sequence in which the bite size of the butadiene ligand decreases continuously, the envelope conformation of the ring becomes increasingly planar, and the free energy of activation for ring inversion decreases. If the sequence of observed structures is interpreted as mapping the reaction pathway and if for a molecule with equilibrium structure x_0 the energy profile along the reaction coordinate x is of the form $\Delta E = ax^4 - 2ax_0^2x^2$, it may be shown that $\Delta E^\ddagger = -ax_0^4$. The experimental data closely follow such a relationship, $\Delta G^\ddagger = -ax_0^4$. This finding establishes a relationship between change in equilibrium structure, change in activation energy, and energy profile for an individual molecule. The results represent a quantitative illustration of Hammond's postulate based exclusively on experimental structural and kinetic data.

Structural Correlations. A commonly used method to gain chemical information is to study a basic molecular fragment in different environments. In particular, variation of substituents provides a basis for discerning electronic and steric effects on the properties of the fragment. This general idea has been applied over the last 15 years to the analysis of changes in structural parameters of molecules containing the same basic fragment. It has been found that changes in distances and angles are often correlated and that this correlation can be interpreted in terms of structural reaction coordinates for such diverse processes as conformational interconversions, bond-breaking and bond-making processes.[1] The influence of varying environments may be considered as a perturbation on the energy surface of the basic fragment,[2] which preserves its basic features of minima, valleys, and transition states. In the last few years both structural and kinetic data have become available for sufficiently large families of related molecules. This opens up the possibility of enlarging the scope of structural reaction pathway studies by adding the dimension of energy. In this paper results of X-ray crystal structure determinations and of temperature-dependent NMR experiments are combined with the aim of understanding an observed, rather pronounced dependence of activation energy on small changes in observed molecular structure.

Automerization of Zirconocene and Hafnocene Complexes. (*s-cis*-η^4-Butadiene)zirconocene and -hafnocene complexes have been investigated and described in the literature by Erker and co-workers.[3-6] Temperature-dependent NMR spectroscopy in solution shows dynamic behavior, which has been interpreted in terms of a ring-inversion mechanism[3,5] (Scheme I). Structural data are available for 12 related compounds,[3-8] 9 zirconocene and

(1) For a review, see: Bürgi, H. B.; Dunitz, J. D. *Acc. Chem. Res.* **1983**, *16*, 153–161.
(2) Or, more accurately, on a reference molecule suitably chosen from a family of related molecules.
(3) Erker, G.; Engel, K.; Krüger, C.; Chiang, A.-P. *Chem. Ber.* **1982**, *115*, 3311–3323.
(4) Erker, G.; Engel, K.; Krüger, C.; Müller, G. *Organometallics* **1984**, *3*, 128–133.
(5) Krüger, C.; Müller, G.; Erker, G.; Dorf, U.; Engel, K. *Organometallics* **1985**, *4*, 215–223.
(6) Erker, G.; Engel, K.; Krüger, C.; Tsay, Y.-H.; Samuel, E.; Vogel, P. *Z. Naturforsch., B: Anorg. Chem., Org. Chem.* **1985**, *40B*, 150–157.

0002-7863/88/1510-4953$01.50/0

Scheme I

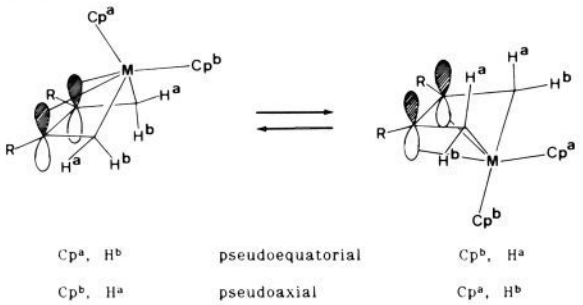

3 hafnocene complexes (Chart I and Table I). The bond distances between M and X1, X4 are short; the distances between M and C2, C3 are distinctly longer and quite variable.

Present Work. In this work, we analyze structural parameters of the metallacyclopentene fragment with the aid of factor analysis.[9] The purpose of the statistical analysis is to find a model for the reaction coordinate of the automerization process. The coordinate is correlated with experimental activation energies; a small structural change toward the transition state, induced by changing the substituents on the *s-cis*-η^4-butadiene ligands, is found to concur with a large change in activation energy. It is shown that the structure–energy correlation is consistent with a symmetric double-well potential for ring inversion and a simple quadratic perturbation to account for the change in substituents. The correlation and its interpretation in terms of potential energy provide quantitative illustration of Hammond's postulate.[10]

Results

Principal-Component Analysis[11] of Six (Scaled) Internal Coordinates. The structure of the metallacyclopentene molecular fragment was analyzed in terms of the M–X, M–C, X–C, and C–C distances and the X–C–C angle β and the dihedral angle $\theta 1$, both scaled to length units (Figure 1). Details of data retrieval, data processing, and subsequent analyses are given in an appendix (supplementary material). The mean values of the structural parameters and their ranges (expressed as a standard deviation) are given in Table II. The changes in these parameters on going from one molecule to another are highly correlated. The details of these correlations are deduced by principal-component analysis, as listed in Table II and shown in Figure 2. The analysis shows that the structural variability of the metallacyclopentene fragment may be described in terms of only two coordinates rather than the original six. One of them (PRIN1 in Table II) is an inversion coordinate, and it is identical with the internal coordinate $\theta 1$ (Figure 3, top); the other is a mixture of mainly two of the remaining five coordinates, namely the M–C distances and the angle β (PRIN2 in Table II). It measures the bite size of the organic ligand. As the distance M to C increases, the angle β decreases while $\theta 1$ remains constant (Figure 3, bottom).

These two coordinates account for 99.9% of the total structural variance; the contribution of the first one amounts to 97.7% and

Chart I

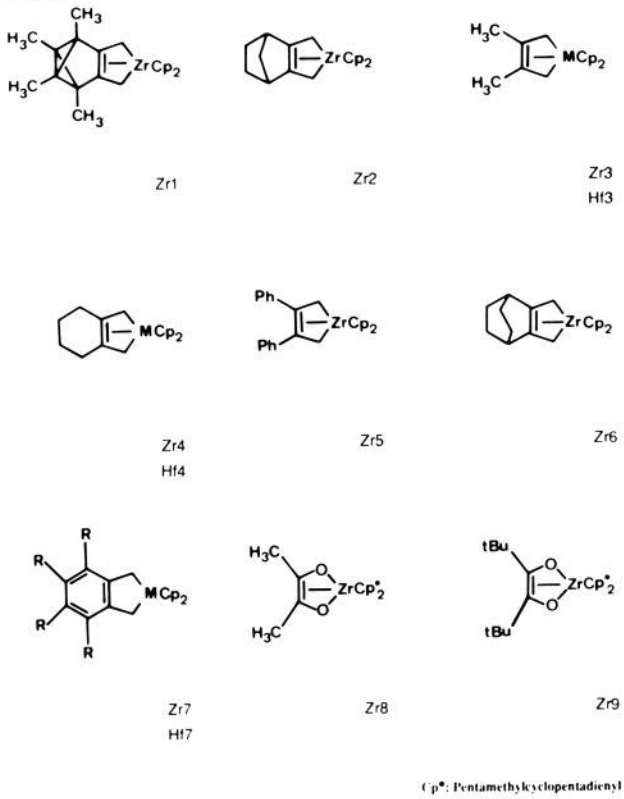

that of the second one to 2.2%. The third principal component with an eigenvalue of only 0.002 Å^2 (0.1%, Table II) comes close to the average experimental variance in distances (~0.000 04 Å^2) and especially in angles (~0.0002 Å^2, scaled to length units). This factor is unlikely to contain much chemical information.

In Figure 2 the 29 observations have been transformed to the new system of coordinates (labeled PRIN1 and PRIN2). The origin of this coordinate system is given by the mean parameter values (Table II). The data points are not randomly distributed in this plane but follow, more or less closely, a curve that initially runs parallel to PRIN2, and then turns around to be parallel to PRIN1 at PRIN1 = 0, and ends up parallel to PRIN2 again. Along PRIN2 the distance M–C2 is elongated by opening the angle β, i.e. by increasing the ligand bite, but keeping the dihedral angle $\theta 1$ unchanged. Later on, this deformation continues but is now accompanied by a gradual flattening of the metallacyclopentene fragment until at $\theta 1 = 0$ (=PRIN1) the molecule is planar.

The coordinate PRIN2 accounts for only 2.2% of the total variance as opposed to 97.7% for PRIN1, indicating that it is unimportant in defining the reaction coordinate. These numbers are misleading, however; they are due to the peculiar distribution of data points (Figure 2) that cluster at PRIN1 $\approx \pm 1.5$ Å but are more or less evenly distributed along PRIN2 between −0.3 and +0.6 Å. This results in a much larger eigenvalue for PRIN1 than for PRIN2 (Table II). In contrast, corresponding ranges are much more similar: ~3 Å for PRIN1 and ~0.9 Å for PRIN2. The coordinate PRIN2 is thus an essential part of the reaction coordinate.

Principal-Component Analysis[11] of the Inertial Coordinates. Analysis of the covariance of inertial coordinates yields a similar picture. Two composite coordinates or factors account for 99.3% of the total variance (Table III of the supplementary material). The first factor contains only the atomic z coordinates and the second one only the atomic x and y coordinates. A graphical representation of the two eigenvectors is given in Figure 3. As before, PRIN1 corresponds to the ring-inversion coordinate, whereas PRIN2 corresponds to elongation of M–C2 and compression of X1–X4. Transformation of the 29 observations to the

(7) Bristow, G. S.; Lappert, M. F.; Martin, T. R.; Atwood, J. L.; Hunter, W. F. *J. Chem. Soc., Dalton Trans.* **1984**, 399–413.
(8) Hofmann, P.; Frede, M.; Stauffert, P.; Lasser, W.; Thewalt, U. *Angew. Chem.* **1985**, *97*, 693–694.
(9) Factor analysis is a method to analyze covariance of multivariate systems. The covariance matrix is transformed to an eigenvector basis ranked according to eigenvalues. Very often some of the smaller eigenvalues account for an insignificant fraction of the total variance, and the corresponding eigenvectors are dropped. The total number of variables is thus reduced to a smaller number of significant factors, which account for most of the variance. For a general reference, see: Malinowski, E. R.; Howery, D. G. *Factor Analysis in Chemistry*; Wiley-Interscience: New York, 1980. For applications in structural chemistry, see: (a) Murray-Rust, P.; Motherwell, S. *Acta Crystallogr., Sect. B: Struct. Crystallogr. Cryst. Chem.* **1978**, *B34*, 2518–2526. (b) Murray-Rust, P. *Acta Crystallogr., Sect. B: Struct. Crystallogr. Cryst. Chem.* **1982**, *B38*, 2765–2771.
(10) Hammond, G. S. *J. Am. Chem. Soc.* **1955**, *77*, 334–338.
(11) *SAS User's Guide: Statistics Version 5 Edition*; SAS Institute: Cary, NC, 1985.

Table I. Selected Structural Parameters of 15 (*s-cis*-η^4-Butadiene)metallocene and Related Molecules and Free Energy of Activation for Automerization (Figure 1)

name	$\Delta G^{\ddagger}_T$[d]	M-X1[e]	M-C2[e]	X1-C2[e]	C2-C3[f]	X1-C2-C3: β[g]	M-X1-C2: γ[g]	$\theta 1$[h]	C2-R[e]	C3-C2-R: α[g]	$\theta 2$[i]	ref
Zr1[a]	14.3 (+11)	2.317	2.550	1.445	1.398	129.6	81.8	56.6	1.522	104.4	8.9	3
Zr11		2.316	2.552	1.447	1.395	129.8	81.9	56.1	1.518	104.6	9.2	
Zr12		2.319	2.549	1.444	1.401	129.5	81.7	57.1	1.527	104.2	8.6	
Zr2		2.318	2.574	1.454	1.391	128.6	82.7	57.7	1.534	106.1	1.6	3
Zr3	11.5 (-42)	2.300	2.597	1.451	1.398	122.7	84.4	67.2	1.511	121.8	7.1	4
Hf3	8.3 (-105)	2.267	2.641	1.472	1.378	121.7	87.2	63.5	1.522	122.1	8.9	5
Zr4[a]	10.8 (-57)	2.279	2.635	1.465	1.379	123.5	86.6	61.2	1.523	120.5	6.1	5
Zr41		2.280	2.625	1.461	1.378	123.4	86.2	62.2	1.527	120.6	5.3	
Zr42		2.279	2.645	1.469	1.379	123.6	87.0	60.2	1.519	120.5	6.9	
Hf4[a]	7.6 (-121)	2.255	2.716	1.470	1.370	121.8	91.2	56.6	1.510	121.0	5.4	5
Hf41		2.263	2.700	1.460	1.370	122.5	90.2	56.6	1.510	121.3	5.9	
Hf42		2.247	2.737	1.480	1.370	121.2	92.3	55.2	1.510	120.8	4.9	
Zr5	8.0 (-112)	2.289	2.714	1.473	1.392	121.3	89.7	60.4	1.505	122.8	4.7	4
Zr6	7.1 (-131)	2.289	2.693	1.472	1.385	125.1	88.7	53.1	1.528	112.7	-1.8	6
Zr7[b]	6.5 (-140)	2.300	2.855	1.480	1.420	119.4	95.8	53.1	1.400	118.0	5.6	7
Hf7[c]		2.279	2.908	1.495	1.413	118.5	98.7	49.3	1.398	118.1	6.3	7
Zr8		2.040	2.829	1.369	1.315	118.0	110.6	16.8	1.524	127.3	2.0	8
Zr9	0.0	2.017	2.938	1.386	1.357	113.9	118.2	0.0	1.533	134.9	1.5	8

[a] Two independant observations. First line, mean values; following lines, individual values. [b] $\Delta G^{\ddagger}_T$ for R = CH_3; structure for R = H (Chart I). [c] Structure for R = H (Chart I). [d] In kilocalories per mole; ^{1}H NMR Cp coalescence temperature in parentheses (°C). [e] In angstroms, mean with respect to assumed molecular mirror plane. [f] In angstroms. [g] In degrees, mean with respect to assumed molecular mirror plane. [h] Dihedral angle in degrees (X1-M-X4, X1-C2-C3-X4). [i] Interplanar angle in degrees (X1-C2-C3-X4, R-C2-C3-R).

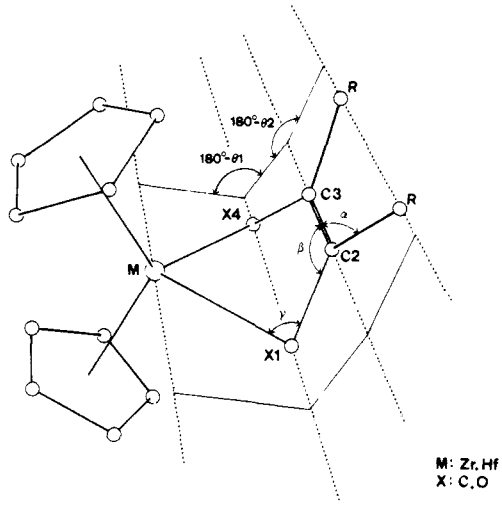

Figure 1. Definitions of structural parameters.

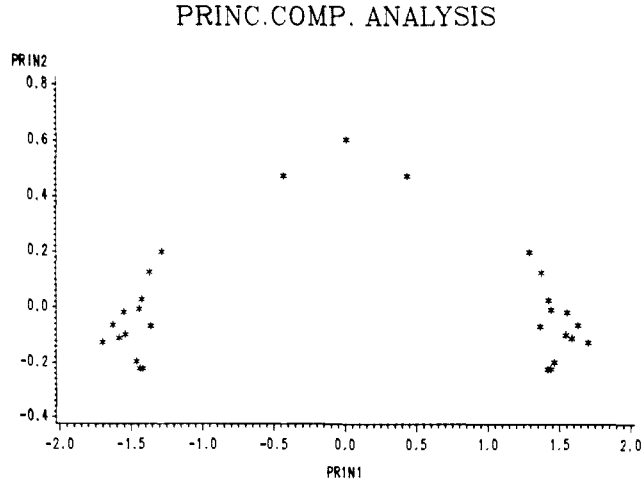

Figure 2. Scaled internal structural parameters projected onto the plane defined by the two most important factors (Å).

plane defined by PRIN1 and PRIN2 yields a distribution almost indistinguishable from that obtained from internal coordinates (Figure 1 of the supplementary material).

Table II. Results of Principal-Component Analysis on Covariance Matrix of Six Structural Parameters

Means and Standard Deviations, Å			
M-X1	2.295 (0.015)	M-C2	2.742 (0.204)
X1-C2	1.468 (0.015)	C2-C3	1.384 (0.025)
β_s	3.148 (0.079)	$\theta 1_s$	0.0 (1.43)

	PRIN1	PRIN2	PRIN3
eigenvalues, Å^2	2.056	0.046	0.002
fraction of total variance	0.977	0.022	0.001
eigenvectors			
M-X1	0	-0.017	0.188
M-C2	0	0.947	0.306
X1-C2	0	0.052	-0.060
C2-C3	0	-0.060	-0.086
β_s	0	-0.311	0.927
$\theta 1_s$	1.0	0	0

Discussion

Structural Correlation and Activation Energies. In line with the concepts referred to in the introduction, the correlation shown in Figure 2 is interpreted as a model of the structural part of the reaction coordinate; it follows that the symmetric structure of compound Zr9 resembles the transition state for the automerization reactions (or that of an energetically high-lying intermediate). With this the dependence of activation energy on the distances between ground states and transition state can be analyzed and interpreted.

The bond length M-C2, the simplest approximation to the reaction coordinate, is related to $\Delta G^{\ddagger}$ for the automerization process (Table I). The compound Zr1 with the shortest distance M-C2(C3), 2.55 Å, shows the biggest automerization barrier (14.3 kcal mol^{-1}), whereas the longest distance M-C2(C3), 3.32 Å, of compound Zr9 concurs with the lowest barrier (~0 kcal mol^{-1}). The following approximate dependence (eq 1) is found.

$$\Delta G^{\ddagger} \approx 50[(\text{M-C2}) - 3.32]^2/2 \text{ (kcal mol}^{-1}) \quad (1)$$

A change of the M-C2 bond length by 0.22 Å, from 2.55 Å (Zr1) to 2.77 Å (mean of Zr6 and Zr7), halves the activation energy. Thus, a relatively small structural change (~30% of the total change of 3.32 - 2.55 = 0.77 Å) correlates with a large energy variation (Figure 4).

For a more detailed picture of the dependence between structure and energy, the simple coordinate M-C2 is replaced by the more complex reaction coordinate derived in previous paragraphs (Figure 2). To obtain distances x_0 between the planar transition-state structure and the observed ground-state structures, the

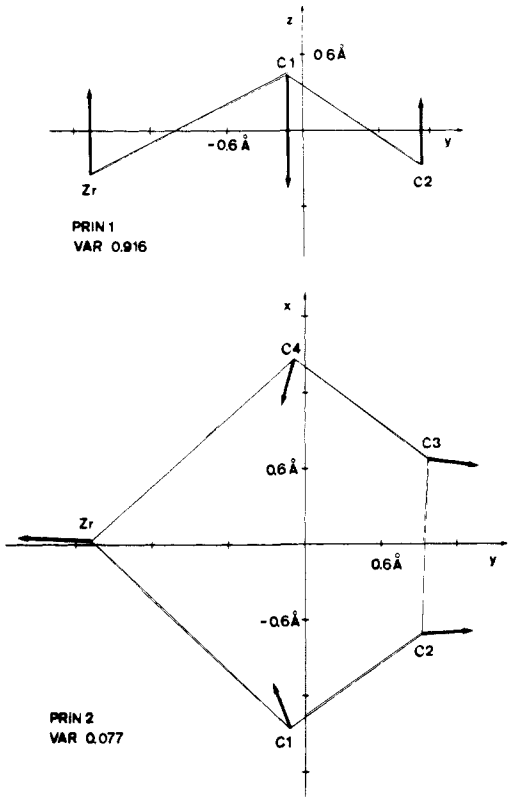

Figure 3. Distortions corresponding to first two principal components (inertial coordinates) applied to the fragment Zr5 (arbitrary absolute magnitudes of displacement vectors).

reaction coordinate (Figure 3) was approximated by four straight-line segments. Very crudely, two of them follow the equations PRIN1 = ±1.4 Å, in the range (PRIN1, PRIN2) from (±1.4 Å, −0.25 Å) to (±1.4 Å, 0.3 Å). The other two are PRIN2 ≈ ±0.21PRIN1 + 0.6 Å in the range from (±1.4 Å, 0.3 Å) to (0 Å, 0.6 Å).

A plot of the distance x_0 along the reaction coordinate[12] versus activation energy is given in Figure 5 together with two interpretations. On the right a quadratic dependence of $\Delta G^{\ddagger}$ on x_0 is assumed, leading to eq 2. On the left of Figure 5 a fourth-order dependence is assumed (eq 3).

$$\Delta G^{\ddagger} \approx 6x_0^2/2 \text{ (kcal mol}^{-1}\text{)} \quad (2)$$

$$\Delta G^{\ddagger} = 0.9x_0^4 \text{ (kcal mol}^{-1}\text{)} \quad (3)$$

The fit is significantly better for eq 3, as shown by the corresponding root-mean-square deviations between observed and calculated energies (1.8 and 1.15 kcal mol^{-1}, respectively).

The trend observed above, namely that the change in activation energy is very steep in the first third of the range of x_0 values, is even more pronounced for the more complex coordinate. In the following section it will be shown how the empirical correlation is related to a simple model of energy surfaces for automerization.

Reaction Profile. The change in energy ΔE along the reaction path for automerization may be expressed tentatively as a double-well potential (eq 4). Equilibrium distance x_0 and barrier height $\Delta E(x_0)^{\ddagger}$ depend on the ratio b/a. They are given in eq 5.

$$\Delta E(x) = ax^4 - bx^2 \quad (4)$$

$$x_0 = \pm(b/2a)^{1/2}$$

$$\Delta E(x_0)^{\ddagger} = -b^2/4a = -ax_0^4 \quad (5)$$

(12) The distance was estimated to be 1.43 + 0.3 − PRIN2 Å.

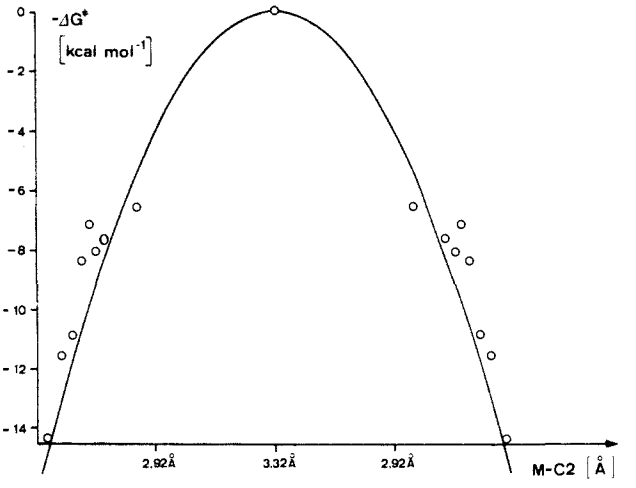

Figure 4. Dependence of free energy of activation on the distance M–C2(C3).

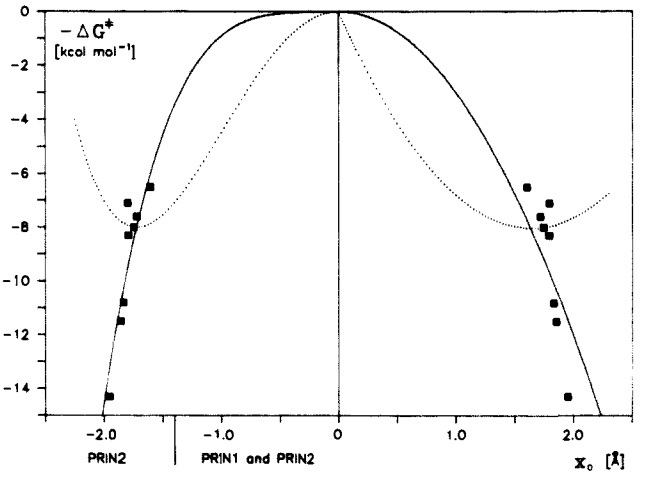

Figure 5. Dependence of free energy of activation $\Delta G^{\ddagger}$ on distance x_0 between ground state and transition state (see text).

The energy profile for an individual molecule is given in eq 6 (Figure 5, left, dotted line), the force constant at equilibrium in eq 7.

$$\Delta E(x) = ax^4 - 2ax_0^2x^2 \quad (6)$$

$$k(x_0) = 8ax_0^2 \quad (7)$$

It follows from eq 5 that barrier height $\Delta E^{\ddagger}$ depends on the fourth power of the distance x_0 and on a quantity a. This is what is observed experimentally, implying that a must be approximately constant for all molecules in the analysis (eq 3 and Figure 5, left, solid line). It is therefore concluded that eq 6 is a reasonable approximation to the reaction coordinate for automerization of a molecule at a distance x_0 from the transition state.

A quadratic function, such as $\Delta E(x) = ax^2 - b|x|$ with $\Delta E(x_0)^{\ddagger} = -ax_0^2$ (eq 2), is clearly insufficient to account for the experimental observations (Figure 5, right, dotted and solid lines).

The difference in energy profiles between two similar molecules characterized by ground states $x_0' = x_0 + \delta x_0$ and x_0, respectively, is

$$\Delta E'(x) - \Delta E(x) \approx -4ax_0\delta x_0x^2$$

It is quadratic in x and expresses the steric and electronic effects due to differences in substitution. The difference is a continuous function, which is zero for the planar transition state and increases on moving toward the ground state. This seems reasonable since the steric interactions between the substituents on C2, C3 and Cp ligands of the metal as well as the interaction of the C2–C3 double bond with the metal are minimal in the planar conformation

but increase upon folding the metallacyclopentene fragment. The observed differences in activation energies may thus be traced to steric and electronic ground-state stabilization ($\delta x_0 > 0$) or destablization ($\delta x_0 < 0$) rather than to a transition-state effect. Note, however, that (de)stabilization affects the reaction coordinate everywhere except at $x = 0$.

Conclusions. Three general conclusions seem to be worth mentioning:

(1) The empirical correlation between ground-state structure and activation barrier (eq 3) is directly related to a model potential (eq 4) describing the energy profile of a given molecule along its way to the transition state. It follows that the correlation between $\Delta E(x_0)^\ddagger$ and x_0 obtained from a series of related molecules provides information on the energy surfaces of individual molecules. Specifically, eq 5 provides force constant information that can be compared to values obtained by independent methods. Here, k is estimated to be ~25 kcal mol^{-1} Å^{-2} (eq 7), which would seem to be reasonable considering the rather long M–C2 distance and the consequent weakness of the bonds. Similar analyses[13] of nondegenerate Ni–O, Ni–N, and C–O bond-breaking reactions yield force constants of ~90, ~120, and ~1000 kcal mol^{-1} Å^{-2}, again in qualitative agreement with vibrational spectroscopic data. Conversely, and probably more important in practice, predictions should be possible on the dependence of reactivity on structure if force constants are known.

(2) The data underlying Figures 4 and 5 represent a quantitative illustration of Hammond's postulate.[10] Contrary to earlier examples of this kind, which dealt with Ni–O, Ni–N,[14] and C–O[15] bond-dissociation reactions, here the transition-state structure is relatively well-defined due to the symmetry of the degenerate reaction. Consequently, the strong dependence of $\Delta G^\ddagger$ on the distance along the reaction path is relatively well established.

(3) The results described would seem to bear on the mode of action of an efficient catalyst. Not only should it bring reactants together in proper orientation, i.e. convert entropy into binding energy of the precursor complex, but it should also induce deformations of the reactants along the reaction coordinate, i.e. convert binding energy into strain energy localized in the reaction coordinate. Even small structural changes in the substrate will have large effects on reaction rates. Quantitative knowledge of the dependence of structure on changes in bonding and nonbonding interactions is thus a prerequisite for engineering such catalysts. This also points to a need for accurate structural information. Since careful diffraction studies are capable of determining atomic positions with a precision of ~0.002 Å, interesting results can be expected in this direction.

Registry No. Hf3, 80161-03-1; Hf4, 93531-46-5; Hf7, 90751-94-3; Zr1, 84079-50-5; Zr2, 75361-79-4; Zr3, 75361-74-9; Zr4, 75361-78-3; Zr5, 75361-77-2; Zr6, 98357-83-6; Zr7, 75070-70-1; Zr8, 110133-05-6; Zr9, 97391-17-8.

Supplementary Material Available: An appendix describing the data processing, the coordinates used in the factor analysis, and the results obtained from internal coordinates (12 pages). Ordering information is given on any current masthead page.

(13) Bürgi, H.-B.; Dunitz, J. D. *J. Am. Chem. Soc.* **1987**, *109*, 2924–2926.

(14) Schwarzenbach, G.; Bürgi, H.-B.; Jensen, W. P.; Lawrance, G. A.; Mønsted, L.; Sargeson, A. M. *Inorg. Chem.* **1983**, *22*, 4029–4038.

(15) Jones, P. G.; Kirby, A. J. *J. Am. Chem. Soc.* **1984**, *106*, 6207–6212.

Reactions of Fe^{II}nta and Fe^{II}edda with Hydrogen Peroxide

J. D. Rush[†] and W. H. Koppenol*,[†]

Contribution from the Department of Chemistry, University of Maryland Baltimore County, Catonsville, Maryland 21228. *Received March 23, 1987*

Abstract: Reactions of ferrous nitrilotriacetate (nta) and ethylenediamine-*N*,*N*′-diacetate (edda) complexes with hydrogen peroxide at neutral pH in the presence of formate lead to transient intermediates characterized by absorptions near 280 and 400 nm as previously observed for hedta as a ligand. The decomposition of hydrogen peroxide by Fe^{III}nta and -edda leads to ligand destruction, which is not inhibited by formate. During this process a reactive intermediate is scavenged by ABTS [2,2′-azinobis(3-ethyl-2,3-dihydrobenzothiazole-6-sulfonate)] at concentrations of the latter that are much higher than expected if the hydroxyl radical were the reactive intermediate. This intermediate is not scavenged by the bromide ion. These stopped-flow and steady-state experiments give evidence for the following reactions (HL = nta, edda): (a) $HLFe^{II} + H_2O_2 \rightarrow HLFe(H_2O_2)$, (b) $HLFe(H_2O_2) + HLFe^{II} + 2H^+ \rightarrow 2HLFe^{III} + 2H_2O$, (c) $HLFe(H_2O_2) + HCO_2^- \rightarrow L^{\bullet}Fe^{II} + CO_2^{\bullet-} + 2H_2O$, (d) $HLFe(H_2O_2) + H^+ \rightarrow L^+Fe^{II} + 2H_2O$, (e) $HLFe(H_2O_2) + ABTS + 2H^+ \rightarrow HLFe^{III} + ABTS^{\bullet+} + 2H_2O$. Reactions b–e are ascribed to a compound designated as $HLFe(H_2O_2)$ in reaction a, which might be a hypervalent iron complex $HLFe^{IV}(OH^-)_2$ but not a hydroxyl radical. The ability of the $HLFe(H_2O_2)$ complex to oxidize ethanol but not bromide suggests a one-electron reduction potential greater than $E^{\circ\prime}(CH_3{}^{\bullet}CHOH,H^+/CH_3CH_2OH) = 1.2$ V at pH 7 and smaller than $E^{\circ}(Br_2^{\bullet-}/2Br^-) = 1.63$ V.

Superoxide anions are produced in vivo (see below) and dismutate to oxygen and hydrogen peroxide. The one-electron reduction of the latter[1] by adventitious metal ions such as Fe^1 and Cu^1 is generally thought to produce the reactive hydroxyl radical. This process is considered to cause oxidative damage. In reactions 1–3 RH is a scavenger and HL is a multidentate ligand for iron

$$O_2^{\bullet-} + HLFe^{III} \rightarrow HLFe^{II} + O_2 \quad (1)$$

$$HLFe^{II} + H_2O_2 + H^+ \rightarrow HLFe^{III} + {}^{\bullet}OH + H_2O \quad (2)$$

$$^{\bullet}OH + RH \rightarrow H_2O + R^{\bullet} \quad (3)$$

[†] Present address: Department of Chemistry and Biodynamics Institute, Louisiana State University, Baton Rouge, LA 70803-1804.

0002-7863/88/1510-4957$01.50/0